Comparative Evaluation of Graphene Nanostructures in GERS Platforms for Pesticide Detection

Swapneel Thakkar, Lidia De Luca, Silvia Gaspa, Alberto Mariani, Sebastiano Garroni, Antonio Iacomini, Luigi Stagi, Plinio Innocenzi, and Luca Malfatti*

Read Online

ACCESS | 📊 Metrics & More | 📖 Article Recommendations | 🔲 Supporting Information

ABSTRACT: Graphene-enhanced Raman scattering (GERS) produces enhancement of the Raman signal, which is based on chemical rather than electromagnetic mechanism such as in the surface-enhanced Raman scattering. Graphene oxide, amino- and guanidine-functionalized graphene oxide, exfoliated graphene, and commercial graphene nanoplatelets have been used to investigate the GERS response with the change of graphene properties. Different graphene nanostructures have been embedded into organic–inorganic microporous films to build a platform for the fast and sensitive detection of pesticides in water. The graphene nanostructures vary in the number of layers, lateral size, degree of oxidation, and surface functionalization. The GERS performances of the graphene nanostructures cast on silicon substrates and embedded in the nanocomposite films have

been comparatively evaluated. After casting a few droplets of the pesticide aqueous solution on the graphene nanostructures, the Raman band enhancements of the analytes have been measured. In the nanocomposite films, the characteristic Raman bands originating from pesticides such as paraoxon, parathion, and glyphosate could be traced at concentrations below 10^{-7}, 10^{-5}, and 10^{-4} M, respectively. The results show that the surface functionalization reduces the GERS effect because it increases the ratio between the sp^3 carbon and sp^2 carbon. On the other hand, the comparison among different types of graphenes shows that the monolayers are more efficient than the few-layer nanostructures in enhancing the Raman signal.
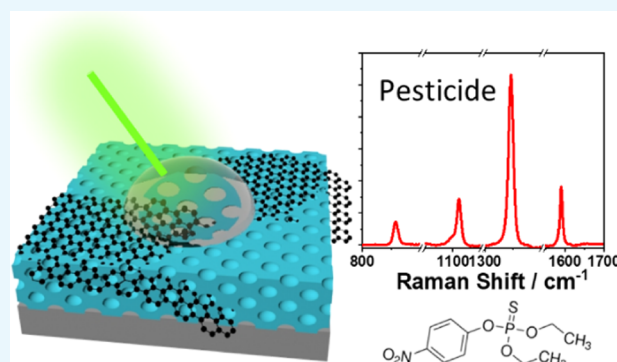
INTRODUCTION

About 2 million tons of pesticides are being utilized globally to increase crop productivity, and in due course of time, they can get accumulated in the ecosystem and enter the food chain, thereby posing a significant threat to human beings.[1,2,4] Trace amount of pesticide is sufficient to cause a significant amount of damage to health;[3] thus, it is essential to build systems to control the excessive use of pesticides and detect them at extremely low concentrations. Conventional analytical techniques such as chromatography, colorimetric, and fluorescence are widely used for qualitative and quantitative assessment of pollutants. Despite being sensitive and accurate, they are expensive, time-consuming, nonportable to the detection site, and often rely on cumbersome processes to preconcentrate the sample before analysis. Therefore, applying tools that are economical, reliable, and eliminate most of the intermediate processes in a single step would be highly desirable for assessing pollutants.

In this regard, Raman spectroscopy can be considered a promising choice to solve all of the challenges presented above. It is a nondestructive technique that requires small sampling volumes, opening the way for the design of microfluidic lab-on-a-chip devices. Despite these advantages, the main limitation of

Raman analysis is the small cross-sectional area for Raman scattering. At extremely low concentrations, the molecular vibrations of the analyte are difficult to detect and require high laser powers combined with a low-noise charge-coupled device (CCD) detector to achieve reliable measurements. One way to increase the intensity of Raman scattering at such concentrations is to utilize a substrate that is coated with noble metallic nanoparticles (NPs). This signal amplification is based on the principle of surface-enhanced Raman scattering (SERS), where the enhancement is both generated by electromagnetic (EM) and chemical mechanism (CM) of interaction between the analyte and the substrate.[5,6] Despite providing high enhancements, there are certain disadvantages in using metallic NPs; they tend to oxidize due to local heating during the SERS detection. For instance, silver NPs are oxidized during the measurements, which makes the measure unreliable due to the
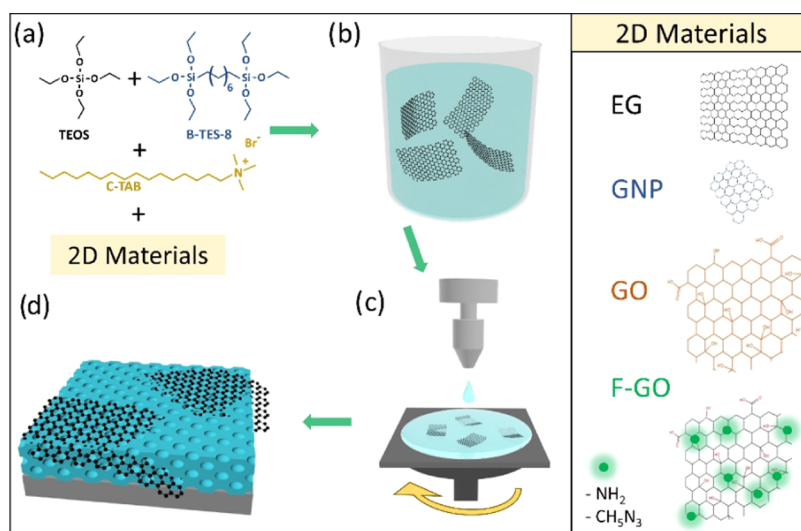
Figure 1. Synthesis of the porous nanocomposite films. (a) Different types of 2D materials (exfoliated graphene, EG; graphene nanoplatelets, GNP; graphene oxide, GO; and functionalized graphene, F-GO) were directly added to the hybrid silica sol (b). (c) The films were prepared by spin-coating (c), which, after thermal treatment, allows the formation of a porous matrix embedding the graphene structures (d).

poor stability of the enhancement after a few days from the synthesis.[5] Utilizing a material to prepare a substrate that does not oxidize and present stable properties over time would be a feasible alternative.

Interestingly, layered materials such as graphene are of great interest as they are stable against photo-induced damage, rely upon the repeatability of measurements after a few days from the synthesis, and provide cleaner molecular vibrations that are free from metal−molecule interactions.[7] The increase in the intensity of analyte molecules using graphene-based materials is termed graphene-enhanced Raman scattering (GERS). Here, the enhancement mainly relies on a chemical mechanism (CM), which involves a direct charge transfer between the analyte and the substrate through $\pi-\pi$ interactions.[7,8] GERS does not perform enhancement by electromagnetic mechanism (EM), as the substrate has a high transmittance (>98%) in the visible range, which does not aid in the absorption of light to generate a plasmon.[7,9] Despite the low peaks' enhancement (up to 10^2 times), the application of graphene and other two-dimensional (2D) materials for GERS has been widely studied because of their cheap and easy synthesis and potential application in flexible devices.

The research to understand the phenomenon of enhancement by graphene is still under debate, as some authors report an enhancement due to fluorescence quenching,[10] while others attribute the effect to resonant Raman conditions.[11] Overall, most of the works have been devoted to studying the GERS effect as a function of the analyte molecular configuration and its number of layers,[6,12] graphene structure, and laser excitation.[7] However, they are described on highly controlled and ideal systems, typically made of organic molecules evaporated on monolayer or few-layer graphene under vacuum conditions.[13−15] These conditions are far from practical applications and standard analytical conditions, which require a robust and reusable detection protocol.

When graphene nanostructures are employed for GERS detection of a liquid sample and ambient conditions, an analyte is deposited on a graphene substrate to enhance the close proximity of Raman signals. Despite the ease of processing, the carbon materials are not utilized to their maximum potential

due to their aggregation issues at solid states because of the strong van der Waals interactions.[16] The aggregation compromises the total surface area of the sheets and limits the availability of active sites, decreasing the probability of capturing analyte molecules. Furthermore, the detection area is usually limited by the laser spot size, and detecting the analyte peaks may be difficult due to the presence of large aggregates. These issues can be solved by dispersing the graphene materials as fillers in a porous matrix avoiding their aggregation at solid states.[17−19] Additionally, in a three-dimensional (3D) porous GERS-active substrate, the probed region is extended to a volume defined by the laser spot size, the porous film thickness, and the laser penetration depth. This increases the probability of the probing analyte molecules and increases the sensitivity of the substrates.

In such a case, silica matrices are apt for developing porous substrate materials due to their low toxicity, high thermal stability, high surface area, robustness, and tunable textural and pore features. These substrates are developed using the sol−gel technique, which additionally allows incorporating fillers such as carbon-based materials. In recent years, our group has developed methods for the synthesis of such hybrid films with controlled features that were investigated for the removal of oil from water,[20] photocatalytic activity,[21] and detection of pesticides/dyes.[22−25] In the case of detection of pollutants, the hybrids enhance the Raman signals due to two synergistic effects: (i) CM offered by the graphene nanostructures, and (ii) pore availability and increased surface area offered by the matrix for the analyte concentration. All of these studies have been reported in our previous findings for sensing dyes and organic pollutants.[22−25] Furthermore, we also developed methods to improve the sensing of these films using the molecular imprinting approach on the porous hybrid films. This provides recognition sites for the analyte molecules to dock onto the active sites of the substrates.[22−24] However, molecular imprinting methods are usually restricted to only one type of analyte rather than a range of target molecules. To extend the field of application on a large variety of analytes, we explore the potential of modifying the characteristics of

graphene nanostructures, such as shape, dimension, number of layers, and defects.

In this work, we have tried to take a step toward the development of a GERS-based detection technology by studying the influence of aggregation and chemical functionalization of graphene layers embedded into porous silica matrixes to detect organic pesticides. This task has been achieved using five different types of graphene nanostructures, namely graphene oxide (GO), guanidine-functionalized-GO (F-GO_Gn), amine-functionalized-GO (F-GO_Am), exfoliated graphene (EG), and graphene nanoplatelet (GNP). The nanocomposite films containing these graphene nanostructures have been then used to detect five types of organophosphate pesticides differing in functional groups and chemical structures.

■ RESULTS AND DISCUSSION

The main purpose of this work is to investigate how different properties of the graphene nanostructures in nanocomposite films affect Raman enhancements (GERS) for different pesticides, used as analytes, cast over the surface of the film.

To achieve this goal, commercial graphene materials (i.e., GO, EG, GNP) and functionalized graphene materials (F-GO-Gn, F-GO-Am) have been embedded in microporous hybrid silica films through solution processing. The commercial GO was functionalized to understand if chemical functionalization is capable of increasing the interactions with organophosphates, which could increase the Raman signals for pesticide sensing. GO has therefore been modified by amino groups to recognize pesticides through noncovalent interaction, or guanidinium groups, to exploit the high affinity for the phosphate groups of organophosphates (such as paraoxon and glyphosate).

The choice of organic−inorganic silica precursors allows the formation of a flexible matrix that is mechanically robust and facilitates the diffusion of the liquid analyte in the porous structure. After synthesis, the nanocomposite films have been used for the GERS detection of five different pesticides. The overall schematic of the synthesis of hybrid films is illustrated in Figure 1.

Characterization of Graphene Nanostructures. The X-ray diffraction (XRD) patterns of the five different graphene nanostructures in Figure 2 show remarkable differences. GO exhibits a quite broad peak at 11.3° with an interlayer spacing of ∼0.86 nm. This diffraction peak is typically associated with a partially aggregated structure with oxidized graphene layers bearing hydroxyls and intercalated water molecules. The peaks
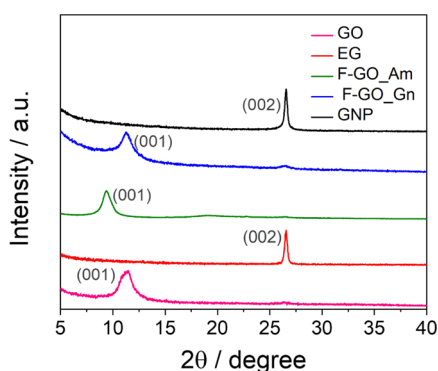
do not shift even after functionalizing GO with guanidium and 1,3-diaminopropane, indicating that the crystalline structure is not affected by the surface modification process. However, it is interesting to observe that the (001) peak of amine-modified GO falls at a lower 2θ value (9.5°) than the amino-functionalized GO, and consequently, the interlayer distance is larger (∼0.94 nm) than that for GO because of the functional group exchange, in accordance with previous findings.[26] EG and GNP, which have not been subjected to any chemical oxidation process, when dried for the XRD analysis, display a sharp peak at 26.6° ascribed to the (002) peak of graphitic carbon.[27]

The presence of surface functional groups on GO and its functional derivatives have been assessed by Fourier transform infrared (FT-IR) spectroscopy, and the spectra are shown in Figure S1. As expected, GO displays several bands (1048, 1235, 1362, 1616, 1725, and 3376 cm^{-1}) which are attributed to the functional groups formed during the oxidation process (C−O, C−O−C, C−O−H, C=C, C=O, and O−H groups, respectively). After chemical modification with amino groups and guanidine, the FTIR spectra of GO also show the bands that are attributed to −NH$_2$ groups from guanidium and 1,3-diaminopropane.

Raman spectroscopy has been used to characterize all of the graphene nanostructures. Figure 3 shows typical spectra of graphene materials that display 3 main peaks: the D band and 2D bands at around 1350 and 2720 cm^{-1}, and the G band at around 1580 cm^{-1}. Information such as the level of strain, doping, crystallinity, and the number of layers can be extracted by examining the G and 2D bands, while the lattice defects can be studied from the D band, which also includes the information on the sp^3-hybridized carbon during functionalization.[28] From Figure 3a, the increase in the intensity of the D band in F-GO_Gn and F-GO_Am indicates functionalization and formation of the sp^3-hybridized bonds during the chemical modification of GO, whereas the intensity and the position of the 2D band do not change, indicating that surface modification does not alter the structural properties of the material upon functionalization.

The 2D band in EG appears asymmetric and is formed by 2 components: a first peak at 2718 cm^{-1} and a second band, identified as a shoulder, around 2680 cm^{-1}. The shape and position of the 2D band in EG indicate the presence of few-layer aggregates in accordance with previous findings.[29] On the contrary, the 2D band of GNP is centered at lower wavenumbers and can be easily deconvoluted with one Lorentzian curve. This approach helps in describing the nature of the layered structure (monolayers or n-layers) of the embedded graphene nanostructures (Figure 3b,c). The Raman spectrum of GNP indicates that graphene is in form of monolayers, in agreement with the specifications of the material provided by the manufacturer.

The quantification of disorder and defect density of the nanostructures can be obtained by calculating the ratio between the D band and G band; the intensity is normally used to estimate this ratio as it represents the phonon modes or molecular vibrations. I_D/I_G has been calculated for all the samples and is displayed in Figure 4. The increase of the I_D/I_G value is due to the high intensity of the D peak, which indicates the breaking and transformation of sp^2 bonds to form sp^3 bonds. From the table of Figure 4d, it is clear that the functionalization of graphene oxide causes a remarkable increase of the sp^3/sp^2 C atomic ratio, which is from 20% to
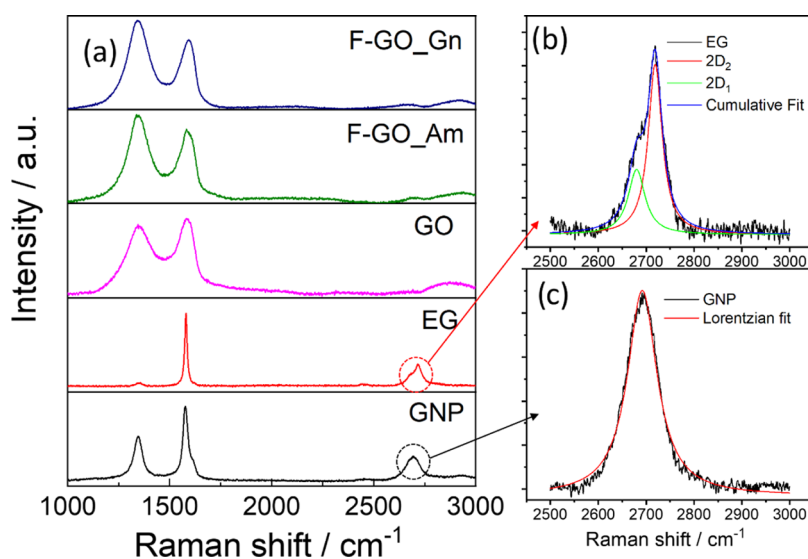

Figure 2. XRD pattern of graphene nanostructures.

Figure 3. (a) Raman spectra of different graphene nanostructures, and Lorentzian fit of (b) EG and (c) GNP.

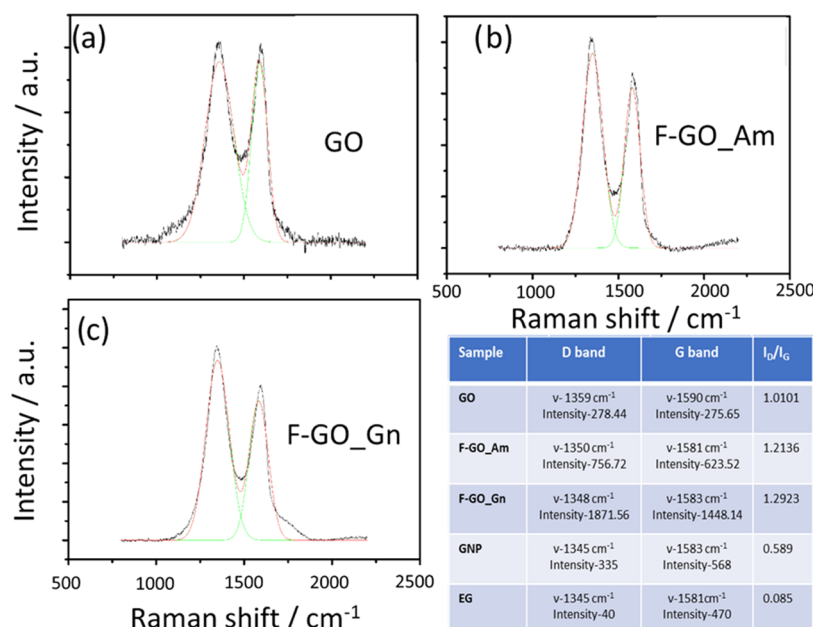| Sample	D band	G band	I_D/I_G
GO	v- 1359 cm⁻¹ Intensity-278.44	v- 1590 cm⁻¹ Intensity-275.65	1.0101
F-GO_Am	v- 1350 cm⁻¹ Intensity-756.72	v- 1581 cm⁻¹ Intensity-623.52	1.2136
F-GO_Gn	v- 1348 cm⁻¹ Intensity-1871.56	v- 1583 cm⁻¹ Intensity-1448.14	1.2923
GNP	v- 1345 cm⁻¹ Intensity-335	v- 1583 cm⁻¹ Intensity-568	0.589
EG	v- 1345 cm⁻¹ Intensity-40	v- 1581cm⁻¹ Intensity-470	0.085

Figure 4. Peak fit of (a) GO, (b) F-GO_Am, and (c) F-GO_Gn. The green lines are the Lorentzian curve used for fitting, while the red lines are the cumulative fit. (d) the table with I_D/I_G values of graphene nanostructures.

almost 30% higher than that in GO. This evidence suggests that the amino-based functions can induce dramatic changes in the GO structure, likely causing significant changes in the GERS. On the contrary, the I_D/I_G ratio of the EG Raman spectrum is close to zero, indicating that the large majority of the C atoms in the structure show sp² hybridization. The ratio is one order of magnitude higher in GNP, suggesting a higher number of defects in these materials with respect to EG. In 2D layered materials, the defect can be located both on the surface of the material or at the edges of the layers. In other words, a difference in the lateral size of the sheets could be responsible for an increase in the I_D/I_G ratio as well as a higher degree of oxidation.

To clarify whether the lateral size of the graphene nanostructure could play a role in determining the I_D/I_G ratio, we have studied the material's morphology by transmission electron microscopy (TEM), as shown in Figures 5

and S2. The 2D nanostructures sensibly differ in lateral sizes; GO, F-GO (both Am and Gn) and EG reveal average lateral sizes of ∼2.7, 2.5, and 2.3 μm, respectively, while the dimension of GNP is below the micron, in the range of ∼0.6 μm.

Among all of the samples, GO shows the largest size as it has been directly processed from graphite by the chemical route. The chemical modifications to prepare F-GO samples do not seem to significantly affect the lateral size. On the contrary, the process to produce GNP gives much smaller flakes, whose size can justify the relatively high I_D/I_G with respect to EG.

Characterization of Hybrid Nanocomposite Films. The design of the host material for GERS sensors in the shape of porous films is of crucial importance. We have designed the hybrid by co-hydrolysis of a silicon alkoxide and a bridged silsesquioxane, which allows obtaining a mechanically flexible and robust material and could easily incorporate different types
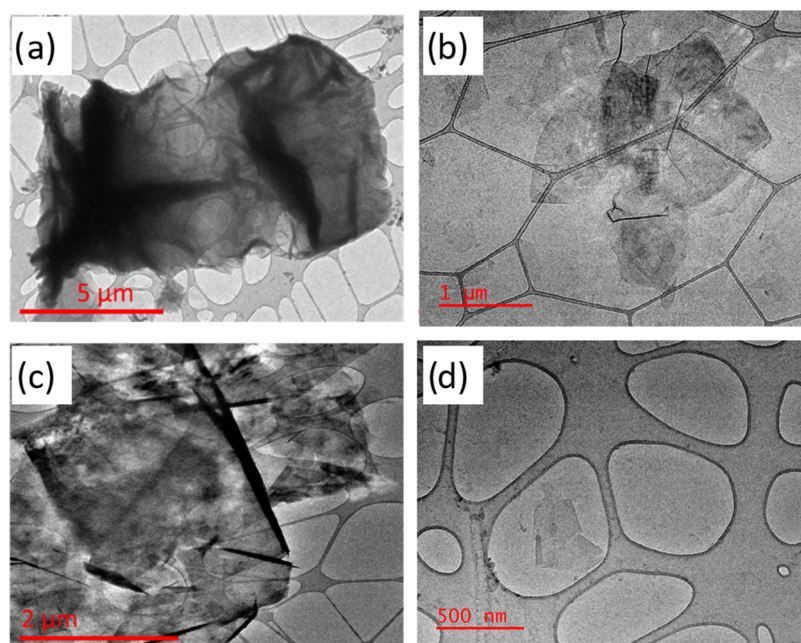
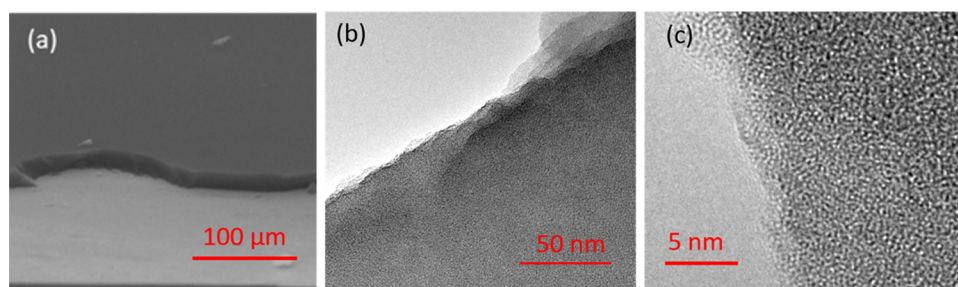**Figure 5.** TEM micrographs of GO (a), F-GO_Am (b), EG (c), and GNP (d).

Figure 6. SEM image showing the film thickness of mSiO$_2$_GNP (a); TEM characterization of the microporous structure of these films (b, c).

of graphenes. The porosity in the films has been generated using an ionic surfactant such as CTAB, as a micropore template. This approach enables the fabrication of the hybrid nanocomposite silica films with a 20% porous volume, as previously reported.[25] After the film deposition, the surfactant molecules were removed by treating the samples at 150 °C for 1 h, leaving behind micropores. After the synthesis, the graphene nanostructures embedded in the hybrid films have been assessed for defects using Raman spectroscopy. The I_D/I_G ratio of graphene nanostructures in the films (Figure S3) showed similar values as their prepared states, which indicates that no significant amounts of defects have been introduced in the graphene nanostructures during fabrication, as expected and previously observed.[21] The thickness of the hybrid films has been estimated by spectroscopic ellipsometry to be 1.1 ± 0.08 μm and does not show a significant difference as a function of the type of graphene nanostructure embedded in the matrix. The thickness values were also assessed by measuring the cross section of the film by scanning electron microscopy (SEM), and Figure 6a describes the thickness of mSiO$_2$_GNP in the range. Furthermore, TEM analysis of this film reveals their inner microporous structure; as expected, the hybrid films have shown a homogenous and not-organized porous structure with pore sizes less than 1 nm (micropores) as shown in Figure 6b,c, which is also similar to other hybrids of this work and our previous findings.[23,24]

Enhancement of Peaks. The efficiency of a SERS or GERS substrate is often assessed by evaluating the amplification generated by molecules adsorbed onto the Raman-active substrate with respect to noninteracting supports. The analytical enhancement factor (EF) is then calculated as a ratio of the selected band intensities taken from the Raman spectra of active and nonactive substrates divided by the number of molecules involved in the measurement. In this work, however, we have considered the ratio (I/I_0) of selected Raman band intensities of the pesticides' aqueous solution measured after casting the liquid on a flat silicon wafer with no coating and on porous silica/graphene films. The plain porous Si film acts as a reference to estimate the enhancement produced by the microporous substrate in comparison with the flat silicon and graphene fillers.

Five pesticides featuring different chemical groups and structures (paraoxon-ethyl and paraoxon-methyl, parathion-ethyl and parathion-methyl, and glyphosate) have been used as the analyte to check the detection limit of the GERS on the films. At first, the pesticides have been diluted in water at decreasing concentrations and directly measured by Raman spectroscopy by casting the solution on a flat silicon wafer (Figures S4 and S5). Then, the same solutions have been cast on the graphene nanostructures and nanocomposite films. Using this approach, paraoxon, parathion, and glyphosate could be traced at concentrations below 10^{-7}, 10^{-5}, and 10^{-4}
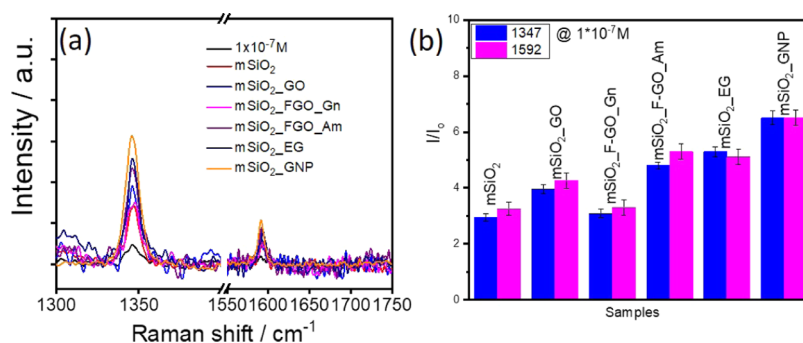
Figure 7. (a) Raman spectra of paraoxon ethyl solutions (10^{-7} M concentration) cast on the nanocomposite films (the black line refers to the solution cast on bare silicon, while the red line refers to the hybrid microporous silica film, mSiO$_2$). (b) Raman amplification of different nanocomposite films as calculated by dividing the band intensity at 1347 and 1592 cm^{-1} of the paraoxon ethyl Raman spectrum deposited on a flat silicon substrate with the intensity of the same band measured.

M, respectively, with a fast and reproducible method. After the measurements, the hybrid films can be washed with water, dried under air, and re-used for further measurements. The difference in the detection limits is mainly due to the intrinsic difference in the scattering efficiency of the pesticide compounds. Figure 7a shows the Raman spectra measured from a 10^{-7} M paraoxon ethyl water solution deposited over a flat silicon substrate, hybrid porous silica, and nanocomposite substrates containing five different types of graphenes. The spectra at higher concentrations are also reported in Figure S6. The bar plot in Figure 7b allows clarifying the amplification provided by the substrates. The plot has been obtained by comparing the maximum intensities (I_o) of the paraoxon ethyl Raman bands (at 1347 and 1592 cm^{-1}, respectively) when the pesticide is deposited on a flat and not-interacting silicon wafer, with the maximum intensity (I) of the same band when the paraoxon ethyl is deposited on a porous nanocomposite. First of all, the effect of the microporous silica matrix (mSiO$_2$) is that of intensifying the Raman band by a factor of 3. This effect is due to the increase of the surface area, which allows exciting a larger number of pesticide molecules using the same spot size. It is important to stress that the increase of the Raman band intensity of mSiO$_2$ is not due to a higher enhancement factor (EF) but rather to a higher number of molecules involved in Raman scattering, as previously observed.[25] The use of a microporous matrix is capable of absorbing the analyte within the whole thickness and therefore guesting a larger number of molecules in the voids.

When the graphene nanostructures are added to the porous silica film, the enhancement is in general higher, thanks to the GERS effect. This can be clearly observed by comparing the I/I_0 ratio of the mSiO$_2$ sample with those of the nanocomposites samples (Figure 7b). Such a comparison allows revealing, in fact, the so-called analytical enhanced factor (AEF) of the nanocomposite matrices, according to the following formula

$$\text{AEF} = \frac{I_{\text{ERS}}}{I} \times \frac{h \times P \times \text{LSS}}{h_{\text{ERS}} \times P_{\text{ERS}} \times \text{LSS}} = \frac{I_{\text{ERS}}}{I} \times \frac{h \times P}{h_{\text{ERS}} \times P_{\text{ERS}}} \tag{1}$$

where I is the Raman intensity, I_{ERS} is the intensity given by enhanced Raman scattering, P is the film porosity, h is the film thickness, and LSS is the laser spot size. Based on the spectroscopic measurements and previous findings, we can assume that neither the film thickness nor the porosity is affected by the addition of the graphene nanostructures, allowing the simplification of (1) as follows

$$\text{AEF} = \frac{I_{\text{ERS}}}{I} \times \frac{h \times P}{h_{\text{ERS}} \times P_{\text{ERS}}} \sim \frac{I_{\text{ERS}}}{I} \tag{2}$$

Both the I/I_0 ratio and the AFEs obtained from each nanocomposite film are different and can be attributed to the functional properties of the different types of graphene. The GO and the functionalized GO appear to be less efficient than the EG and the GNP to enhance the Raman signal of the pesticide. This can be ascribed to the high I_D/I_G ratio, suggesting that a loss of sp^2 C is detrimental for the GERS effect. However, this cannot be the only parameter to be considered because it cannot explain the relative difference in amplification among GO, F-GO_Gn, and F-GO_Am. We attribute these differences to different chemical affinities of the functionalized graphenes to paraoxon ethyl. The differences become less significant when we consider the enhancement of other organophosphorus pesticides (Figure S6). The highest enhancements are exhibited by EG and GNP, which show the lowest I_D/I_G ratios. However, also for EG and GNP, the I_D/I_G ratio cannot be the only parameter to be considered. As previously shown, GNP has a lower sp^3/sp^2 ratio but provides higher enhancement. We attribute the performance of this system to the graphene in form of monolayers. The analysis of the 2D band of GNP and EG, in fact, has already shown that EG is mainly formed by few-layer graphene with low defects, while GNP is the only sample that is made by single-layer nanostructures.

Until now, only a few papers that have focused on the dependence between the number of graphene layers and GERS have been published. It has been shown that when an organic molecule, such as an organophosphate, is adsorbed on a graphene layer, it causes a strong chemical doping of the graphene structure because of charge transfer.[30] In fact, the interactions between the analyte and graphene change its Fermi level. Therefore, the molecules adsorbed on the graphene surface act as doping chemical elements. This phenomenon, in turn, is also responsible for the chemical mechanism underlying the GERS. The chemical doping, however, becomes less and less effective as the number of graphene layers increases. The lower Raman enhancement observed in the nanocomposite films containing few-layer graphene is therefore correlated with the graphene thickness (i.e., the number of layers in the graphene nanostructures). However, it is important to note that most of the scientific articles published on the GERS effect report Raman experiments on very simple systems, typically made of organic

molecules evaporated on mono- or few-layer graphene under vacuum conditions. In the present case, the macroscopic GERS effect has been studied in a complex system, i.e., a nanocomposite matrix embedding graphene nanostructures. Although this is a step forward to the engineering of real-world devices, the molecular density of the analyte on the graphene surface is still difficult to control and, therefore, the molecular coverage on the graphene nanostructures could also be considered as the reason for reduced GERS of exfoliated graphene in comparison to graphene nanoplatelets.

The I/I_0 ratios obtained when Raman analysis is performed on graphene nanostructures appear very similar for different pesticides (Figure S7). Therefore, we can average the measurements obtained from different analytes to construct an overall bar plot of the Raman enhancements, as shown in Figure 8.
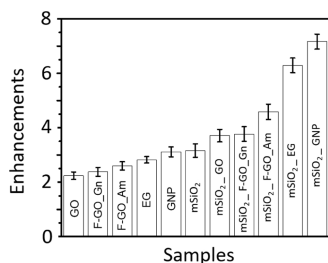

Figure 8. Raman signal enhancements of analyte molecules deposited on different sensing platforms.

■ CONCLUSIONS

Incorporating graphene into a microporous hybrid organic—inorganic films allows the fabrication of an efficient sensing platform to detect the traces of pesticides in water through graphene-enhanced Raman scattering. The Raman response by GERS depends on the chemo-physical properties of graphene, which drastically affect the detection of analytes. The enhancements of Raman bands of pesticides, used as testing molecules, measured on graphene substrates increased 2 to 4 times when incorporated into the microporous matrices. The porous structure of the hybrid organic—inorganic matrix has a double role of separating the graphene flakes and concentrating the analyte. The microporous films combine graphene and analytes in the pores while providing mechanically robust and chemically stable sensing platforms.

The GERS response depends on the type of graphene, which is employed in accordance with the nature of the effects generated by the analyte's chemical interaction with the graphene surface. Graphene nanoplatelet-loaded films have shown the highest Raman enhancement followed by exfoliated graphene and multilayered nanostructures with a higher degree of oxidation, i.e., F-GO_Am, GO, and F-GO_Gn. The results suggest that the chemical functionalization of graphene with specific functional groups is not an effective method to enhance the Raman signal of analyte molecules. On the contrary, the single-layer graphene nanostructures, i.e., GNP, are good candidates to fabricate sensing platforms with fast detection capability. By coupling Raman spectroscopy with the nanocomposite films, paraoxon, parathion, and glyphosate could be traced at concentrations below 10^{-7}, 10^{-5}, and 10^{-4} M, respectively. We expect that the design of proper plasmonic nanostructures to be embedded in the GNP-loaded hybrid

films can further increase the sensitivity of the substrate by several orders of magnitudes by the electromagnetic mechanism.

■ EXPERIMENTAL SECTION

Materials. Tetraethoxysilane (TEOS, Sigma-Aldrich, >99% purity), 1,8-bis(triethoxysilyl)octane (B-TES-8, 97% purity), cetyl trimethyl ammonium bromide (CTAB, Sigma-Aldrich, 99% purity), ethanol (EtOH, >99.8% purity), graphene oxide (GO, Sigma-Aldrich), exfoliated graphene (EG, Sigma-Aldrich), graphene nanoplatelets (GNP, Sigma-Aldrich), hydrochloric acid (HCl, Sigma-Aldrich, 37% wt/wt), para-oxon-methyl, paraoxon-ethyl, parathion, parathion-methyl, and glyphosate were purchased from Sigma-Aldrich and were used as received without further purification. (2-(2-Aminoethyl)-1,3-di-Boc-guanidine) (guanidinium, Sigma-Aldrich, 90% purity), 1,3-diaminopropane (Acros, 99% purity), 1-(3-dimethylaminopropyl)-3-ethylcarbodiimidehydrochloride (EDC*3HCl Alfa Aesar, >98% purity), N-hydroxysuccinimide (NHS, ACROS, >98%) and dimethylformamide extra dry (DMF, Carlo Erba) were utilized to functionalize GO. Silicon wafers were employed as substrates for film deposition; before their use, they were washed with water, acetone, and ethanol and then dried with compressed air and thermally treated at 600 °C in an oven for 1 h. The substrates were cut in dimensions 2 × 2 cm² were then pretreated with a solution ($H_2O/H_2O_2/NH_3 \cdot H_2O$ = 5:1:1) before film deposition.

Synthesis. *Amine-Functionalized GO (F-GO_Am).* A solution of GO sheets (0.140 g) in dry DMF (35 mL) was sonicated in a water bath for 24 h.[28] NHS (1.95 g) and EDC*3HCl (3.28 g) was added to the solution at 0 °C and stirred for 2 h. Then 1,3-diaminopropane (2.17 mL) was added, and the reaction was stirred overnight at room temperature. Later, the mixture was filtered and washed three times with water and ethanol. The GO sheets modified by 1,3-diaminopropane were dried at 40 °C in a vacuum.

Guanidine-Functionalized GO (F-GO_Gn). GO sheets (0.040 g) were added to 40 mL of dry DMF.[29] After 10 min of sonication in a water bath, 2-(2-aminoethyl)-1,3-di-Boc-guanidine (0.970 g) was added to the solution at 0 °C. The mixture was stirred at room temperature for 5 days. Then, GO sheets modified were separated through centrifugation at 4500 rpm for 5 min. DMF was added to the precipitate, sonicated for 5 min, and centrifuged. This work-up step was repeated twice with DMF, MeOH, and DCM. After guanidine functionalization, GO was dried at 40 °C under vacuum.

Deposition of Nanocomposite Films. The preparation of hybrid films was based on our previous report.[22] Briefly, 8 mL of EtOH, 1 mL of TEOS, 2.126 mL of B-TES-8, 0.3 mL of DI water, and 0.05 mL of 1 M HCl were added in a glass vial (molar ratios: TEOS/B-TES-8/EtOH/water/HCl = 1:1:30:6.4:0.025) under stirring to prepare a sol. After 10 min, 0.02 g of CTAB was dissolved in 0.5 mL of EtOH (molar ratio: TEOS/CTAB = 1:0.012; [Si]/CTAB = 1:0.004) were added to the sol and was then left to react under stirring for 2 h at room temperature. Meanwhile, all of the graphene dispersions were adjusted to a concentration of 1 mg mL⁻¹ and 300 μL of the colloidal solution was added to 5 mL of the sol and kept under stirring for 2 h. The films were then prepared by spin coating; 200 μL of the hybrid sol was deposited on the silicon substrate and the substrate was spun at a rate of 1000 rpm for 40 s and then 500 rpm for 20 s to

prepare uniform film coatings. The substrates were then placed at 60 °C overnight and then treated at 150 °C for 1 h.

Sample Preparation for Raman Detection. First, organophosphorus pesticides such as paraoxon-ethyl, paraoxon-methyl, parathion-ethyl, parathion-methyl, and glyphosate aqueous solutions with different molar concentrations were prepared. About 20 μL of the solution was deposited on bare Si substrate and allowed to dry at ambient conditions, and the Raman spectra were recorded. Next, ERS of the pesticide molecules were studied using the graphene nanostructures and nanocomposite films. Briefly, 10 μL of the graphene suspension (0.05 mg mL^{-1}) was mixed with 20 μL of the pesticide solution; the mixture was then deposited onto Si wafer. In the case of hybrid films, 20 μL of the pesticide solution was deposited directly onto the substrates. The laser was focused on the deposited regions on the substrates, and the Raman spectra were collected in 10 different points and then assessed for measuring the enhancement. The Raman spectra are the average of 10 different measurements performed on the same sample. The error bars reported in figures have been estimated according to the standard deviation of the corresponding dataset.

Characterization. X-ray diffraction (XRD) patterns were collected using a Bruker D8 Discover diffractometer at a power of 40 kV and 40 mA, working with a Cu K$_{\alpha 1}$ target (=1.54056 Å). The patterns were recorded at 2θ angle in the range from 5 to 70° and a step size of 0.02 Å.

FTIR spectra were recorded in a transmission mode between 4000 and 400 cm^{-1} by averaging 128 scans at a resolution of 4 cm^{-1} using an interferometer Bruker infrared Vertex 70v.

TEM images were obtained using an FEI TECNAI 200 microscope working with a field emission electron gun operating at 200 kV. The sample preparation of hybrid was done by scratching the films, dispersing their fragments in ethanol by ultrasonication, and then dropping them onto an ultrathin (<3 nm) holey carbon-coated copper grid before drying them for observations, while for graphene materials, they were directly drop-casted onto the grids.

A Woollam-α spectroscopic ellipsometer with fixed-angle geometry was used to measure the thickness of the films deposited on silica substrates. The thickness was estimated by fitting the experimental model developed using dense hybrid films deposited on the silica substrates; the fit showed an average mean square lower than 0.16. The cross section of the film was measured using a SEM FEI Quanta 200 microscope working in a high vacuum mode. The substrates were cut into small pieces placed obliquely on the sample holder.

Raman analysis was performed with a Bruker Senterra confocal Raman microscope with a laser excitation wavelength of 532 nm, a nominal power of 5 mW, and a 50× objective. The spectra were recorded in the 70−4500 cm^{-1} range, with a resolution of 5 cm^{-1}, with an integration time of 5 s and 6 co-additions.

■ ASSOCIATED CONTENT

ⓢ Supporting Information

The Supporting Information is available free of charge at https://pubs.acs.org/doi/10.1021/acsomega.1c04863.

FT-IR spectra of graphene oxide and functionalized graphene oxide; Raman peak fit of Si_F-GO_Am, Si_F-GO_Gn, and table with I_D/I_G values; further TEM images of EG and GNP; Raman spectra of organophosphorus pesticides in decreasing order of molar concentrations; Raman spectra of glyphosate and its corresponding vibration bands; Raman spectra of paraoxon ethyl solutions of 10^{-6} M concentration casted on the graphene nanostructure and nanocomposite films; EF of different nanocomposite films as calculated by considering the bands at 858, 1114, 1347, and 1592 cm^{-1} of the paraoxon-ethyl Raman spectrum; increase in the intensity of organophosphorus pesticide peaks over different kinds of synthesized substrates (PDF)

■ AUTHOR INFORMATION

Corresponding Author

Luca Malfatti − *LMNT, CR-INSTM, Department of Biomedical Sciences, University of Sassari, 07100 Sassari SS, Italy;* ⓞ orcid.org/0000-0001-6901-8506; Email: luca.malfatti@uniss.it

Authors

Swapneel Thakkar − *LMNT, CR-INSTM, Department of Biomedical Sciences, University of Sassari, 07100 Sassari SS, Italy*

Lidia De Luca − *Department of Chemistry and Pharmacy, University of Sassari, 07100 Sassari, Italy;* ⓞ orcid.org/0000-0001-7211-9076

Silvia Gaspa − *Department of Chemistry and Pharmacy, University of Sassari, 07100 Sassari, Italy*

Alberto Mariani − *Department of Chemistry and Pharmacy, University of Sassari, 07100 Sassari, Italy;* ⓞ orcid.org/0000-0001-8973-4542

Sebastiano Garroni − *Department of Chemistry and Pharmacy, University of Sassari, 07100 Sassari, Italy*

Antonio Iacomini − *Department of Chemistry and Pharmacy, University of Sassari, 07100 Sassari, Italy*

Luigi Stagi − *LMNT, CR-INSTM, Department of Biomedical Sciences, University of Sassari, 07100 Sassari SS, Italy; Department of Chemistry and Pharmacy, University of Sassari, 07100 Sassari, Italy;* ⓞ orcid.org/0000-0002-7238-8425

Plinio Innocenzi − *LMNT, CR-INSTM, Department of Biomedical Sciences, University of Sassari, 07100 Sassari SS, Italy;* ⓞ orcid.org/0000-0003-2300-4680

Complete contact information is available at:
https://pubs.acs.org/10.1021/acsomega.1c04863

Author Contributions

The manuscript was written through the contributions of all authors. All authors have given approval to the final version of the manuscript.

Notes

The authors declare no competing financial interest.

■ REFERENCES

(1) Sharma, A.; Kumar, V.; Shahzad, B.; Tanveer, M.; Sidhu, G. P. S.; Handa, N.; Kohli, S. K.; Yadav, P.; Bali, A. S.; Parihar, R. D.; Dar, O. I.; Singh, K.; Jasrotia, S.; Bakshi, P.; Ramakrishnan, M.; Kumar, S.; Bhardwaj, R.; Thukral, A. K. Worldwide pesticide usage and its impacts on ecosystem. *SN Appl. Sci.* **2019**, *1*, No. 1446.

(2) Rodgers, W. H. The persistent problem of the persistent pesticide: A lesson in environmental law. *Columbia Law Rev.* **1970**, *70*, 567−611.

(3) Vos, J. G.; Dybing, E.; Greim, H. A.; Ladefoged, O.; Lambré, C.; Tarazona, J. V.; Brandt, I.; Vethaak, A. D. Health Effects of Endocrine-Disrupting Chemicals on Wildlife, with Special Reference to the European Situation. *Crit. Rev. Toxicol.* **2000**, *30*, 71−133.

(4) Worldatlas Top Pesticide Using Countries. 2018, https://www.worldatlas.com/articles/top-pesticide-consuming-countries-of-the-world.html.

(5) Schlücker, S. Surface-Enhanced Raman Spectroscopy: Concepts and Chemical Applications. *Angew. Chem., Int. Ed.* **2014**, *53*, 4756−4795.

(6) Malfatti, L.; Falcaro, P.; Marmiroli, B.; Amenitsch, H.; Piccinini, M.; Falqui, A.; Innocenzi, P. Nanocomposite mesoporous ordered films for lab-on-chip intrinsic surface enhanced Raman scattering detection. *Nanoscale* **2011**, *3*, 3760−3766.

(7) Ling, X.; Huang, S.; Kong, J.; Dresselhaus, M. *Recent Developments in Plasmon-Supported Raman Spectroscopy 45 Years of Enhanced Raman Signals*, Kneipp, K.; Ozaki, Y.; Tian, Z.-Q., World Scientific, 2017; pp 415−449.

(8) Ling, X.; Huang, S.; Deng, S.; Mao, N.; Kong, J.; Dresselhaus, M. S.; Zhang, J. Lighting Up the Raman Signal of Molecules in the Vicinity of Graphene Related Materials. *Acc. Chem. Res.* **2015**, *48*, 1862−1870.

(9) Bruna, M.; Borini, S. Optical constants of graphene layers in the visible range. *Appl. Phys. Lett.* **2009**, *94*, No. 031901.

(10) Martyshkin, D. V.; Ahuja, R. C.; Kudriavtsev, A.; Mirov, S. B. Effective suppression of fluorescence light in Raman measurements using ultrafast time gated charge coupled device camera. *Rev. Sci. Instrum.* **2004**, *75*, 630−635.

(11) Barros, E. B.; Dresselhaus, M. S. Theory of Raman enhancement by two-dimensional materials: Applications for graphene-enhanced Raman spectroscopy. *Phys. Rev. B* **2014**, *90*, No. 035443.

(12) Ling, X.; Juanxia, W.; Xie, L.; Zhang, J. Graphene-Thickness-Dependent Graphene-Enhanced Raman Scattering. *J. Phys. Chem. C* **2013**, *117*, 2369−2376.

(13) Valeš, V.; Kovaříček, P.; Fridrichová, M.; Ji, X.; Ling, X.; Kong, J.; Dresselhaus, M. S.; Kalbáč, M. Enhanced Raman scattering on functionalized graphene substrates. *2D Mater.* **2017**, *4*, No. 025087.

(14) Valeš, V.; Drogowska-Horná, K.; Guerra, V. L. P.; Kalbáč, M. Graphene-enhanced Raman scattering on single layer and bilayers of pristine and hydrogenated graphene. *Sci Rep.* **2020**, *10*, No. 4516.

(15) Feng, S.; dos Santos, M. C.; Carvalho, B. R.; Lv, R.; Li, Q.; Fujisawa, K.; Elías, A. L.; Lei, Y.; Perea-López, N.; Endo, M.; Pan, M.; Pimenta, M. A.; Terrones, M. Ultrasensitive molecular sensor using N-doped graphene through enhanced Raman scattering. *Sci. Adv.* **2016**, *2*, No. e160032.

(16) Lee, J. H.; Avsar, A.; Jung, J.; Tan, J. Y.; Watanabe, K.; Taniguchi, T.; Natarajan, S.; Eda, G.; Adam, S.; Castro Neto, A. H.; Özyilmaz, B. van der Waals Force: A Dominant Factor for Reactivity of Graphene. *Nano Lett.* **2015**, *15*, 319−325.

(17) Innocenzi, P.; Malfatti, L. Mesoporous materials as platforms for surface-enhanced Raman scattering. *TrAC, Trends Anal. Chem.* **2019**, *114*, 233−241.

(18) Innocenzi, P.; Malfatti, L.; Lasio, B.; Pinna, A.; Loche, D.; Casula, M. F.; Alzari, V.; Mariani, A. Sol-gel chemistry for graphene-silica nanocomposite films. *New J. Chem.* **2014**, *38*, 3777−3782.

(19) Carboni, D.; Lasio, B.; Alzari, V.; Mariani, A.; Loche, D.; Casula, M. F.; Malfatti, L.; Innocenzi, P. Graphene-mediated surface enhanced Raman scattering in silica mesoporous nanocomposite films. *Phys. Chem. Chem. Phys.* **2014**, *16*, 25809−25818.

(20) Thakkar, S. V.; Pinna, A.; Carbonaro, C. M.; Malfatti, L.; Guardia, P.; Cabot, A.; Casula, M. F. Performance of oil sorbents based on reduced graphene oxide−silica composite aerogels. *J. Environ. Chem. Eng.* **2020**, *8*, No. 103632.

(21) Malfatti, L.; Falcaro, P.; Pinna, A.; Lasio, B.; Casula, M. F.; Loche, D.; Falqui, A.; Marmiroli, B.; Amenitsch, H.; Sanna, R.; Mariani, A.; Innocenzi, P. Exfoliated graphene into highly ordered mesoporous titania films: Highly performing nanocomposites from integrated processing. *ACS Appl. Mater. Interfaces* **2014**, *6*, 795−802.

(22) Jiang, Y.; Carboni, D.; Malfatti, L.; Innocenzi, P. Graphene oxide-silver nanoparticles in molecularly-imprinted hybrid films enabling SERS selective sensing. *Materials* **2018**, *11*, No. 1674.

(23) Carboni, D.; Jiang, Y.; Faustini, M.; Malfatti, L.; Innocenzi, P. Improving the Selective Efficiency of Graphene-Mediated Enhanced Raman Scattering through Molecular Imprinting. *ACS Appl. Mater. Interfaces* **2016**, *8*, 34098−34107.

(24) Carboni, D.; Jiang, Y.; Malfatti, L.; Innocenzi, P. Selective detection of organophosphate through molecularly imprinted GERS-active hybrid organic−inorganic materials. *J. Raman Spectrosc.* **2018**, *49*, 189−197.

(25) Carboni, D.; Lasio, B.; Loche, D.; Casula, M. F.; Mariani, A.; Malfatti, L.; Innocenzi, P. Introducing Ti-GERS: Raman Scattering Enhancement in Graphene-Mesoporous Titania Films. *J. Phys. Chem. Lett.* **2015**, *6*, 3149−3154.

(26) Ederer, J.; Janoš, P.; Ecorchard, P.; Tolasz, J.; Štengl, V.; Beneš, H.; Perchacz, M.; Pop-Georgievski, O. Determination of amino groups on functionalized graphene oxide for polyurethane nanomaterials: XPS quantitation vs. functional speciation. *RSC Adv.* **2017**, *7*, 12464−12473.

(27) Howe, J. Y.; Rawn, C. J.; Jones, L. E.; Ow, H. Improved crystallographic data for graphite. *Powder Diffr.* **2003**, *18*, 150−154.

(28) Malard, L. M.; Pimenta, M. A.; Dresselhaus, G.; Dresselhaus, M. S. Raman spectroscopy in graphene. *Phys. Rep.* **2009**, *473*, 51−87.

(29) Ferrari, A. C. Raman spectroscopy of graphene and graphite: disorder, electron-phono coupling, doping and nonadiabatic effects. *Solid State Commun.* **2007**, *143*, 47−57.

(30) Peimyoo, N.; Yu, T.; Shang, J.; Cong, C.; Yang, H. Thickness-dependent azobenzene doping in mono- and few-layer graphene. *Carbon* **2012**, *50*, 201−208.